Original Article

MOLECULAR METABOLISM

Targeting microbial bile salt hydrolase reprograms bile acid metabolism and ameliorates metabolic dysfunction—associated steatohepatitis in mice

Wenchao Wei[1,5], Radka Graf[2,5], Yanhan Wang[1], Christopher J. Oalmann[2], Jennifer T. Lau[2], Xinyi Wang[1], Melanie Chien[2], Mary C. Conrad[2], Jonah Simon[2], Souradipta Ganguly[1,3], Tomoo Yamazaki[1], Aenne Harberts[1], Sainan Chen[1], Marcos F. Fondevila[1], Debanjan Dhar[1,3], A. Stewart Campbell[2], Rebecca K. Senter[2,*,6], Bernd Schnabl[1,4,,6]**

ABSTRACT

Microbial bile salt hydrolase (BSH) plays a central role in shaping bile acid composition and gut—liver metabolic signaling, yet its therapeutic potential in metabolic dysfunction—associated steatohepatitis (MASH) remains incompletely defined. Here, we evaluated the efficacy of the non-absorbable BSH inhibitor GR-7 in a diet-induced mouse model of steatohepatitis using early and late intervention strategies with different dosing regimens. GR-7 reduced food intake and exerted stage- and dose-dependent therapeutic effects, with early intervention robustly suppressing hepatic fibrosis even at a low dose, whereas late-stage administration of high-dose GR-7 markedly reduced hepatic steatosis and inflammation, as evidenced by decreased liver weight, hepatic triglyceride and cholesterol levels, and plasma ALT. Although late intervention did not result in statistically significant histological reversal of fibrosis, a trend toward improvement was observed, together with suppression of fibrogenic gene expression, suggesting that prolonged treatment may further enhance antifibrotic efficacy. Mechanistically, GR-7 effectively inhibited microbial BSH activity *in vivo*, leading to reduced cecal unconjugated primary and secondary bile acids—including deoxycholic acid and lithocholic acid, which was associated with improved gut barrier integrity and reduced hepatic inflammation. In parallel, BSH inhibition reprogrammed hepatic bile acid metabolism toward activation of the alternative CYP27A1-mediated synthesis pathway, accompanied by reduced food intake, thereby contributing to reduced hepatic lipid accumulation. Furthermore, late-stage high-dose treatment selectively remodeled the hepatic immune landscape rather than fully restoring homeostasis, highlighting immune recalibration as a key component of therapeutic response. Together, these findings identify microbial BSH inhibition as a promising microbiome-targeted therapeutic strategy for MASH.

Published by Elsevier GmbH. This is an open access article under the CC BY license (http://creativecommons.org/licenses/by/4.0/).

Keywords Gut microbiome; Microbiota; Gut-liver-axis; MASH

1. INTRODUCTION

Metabolic dysfunction—associated steatotic liver disease (MASLD) is an increasingly prevalent metabolic disorder, affecting up to 38% of the adult population globally [1]. Its progressive form, metabolic dysfunction—associated steatohepatitis (MASH), is characterized by hepatocellular injury and inflammation, and represents a critical disease stage that predisposes patients to fibrosis, cirrhosis, and hepatocellular carcinoma [2]. Consequently, MASLD/MASH are associated with increased liver-related morbidity and mortality and are a major driver of the rising need for liver transplantation [3]. These significant clinical and societal burdens show the urgent need for effective pharmacological therapies for MASH. In 2024, resmetirom became the first drug approved by the U.S. Food and Drug Administration for the treatment of MASH [4]. As a selective thyroid hormone receptor-β agonist, resmetirom reduces hepatic lipid accumulation

[1]Department of Medicine, University of California San Diego, La Jolla, CA, USA [2]Vertero Therapeutics, Woburn, MA, USA [3]Center for Metabolic and Liver Diseases & Cancer Genome and Epigenetics, Sanford Burnham Prebys Medical Discovery Institute, La Jolla, CA, USA [4]Department of Medicine, VA San Diego Healthcare System, San Diego, CA, USA

[5] Denotes authors contributed equally to this work.
[6] Denotes co-corresponding authors

*Corresponding author. Vertero Therapeutics, MA01801, Suite 5900, Woburn, MA, USA. E-mail: becca@vertero.com (R.K. Senter).

**Corresponding author. Department of Medicine, University of California San Diego, MC0063, 9500 Gilman Drive, La Jolla, CA 92093, USA. E-mail: beschnabl@ucsd.edu (B. Schnabl).

Received June 1, 2026 • Revision received August 3, 2026 • Accepted August 12, 2026 • Available online 18 August 2026

https://doi.org/10.1016/j.molmet.2026.102430

and improves liver inflammation as well as moderate to advanced fibrosis, representing a major milestone in MASH therapeutics [5]. In addition, semaglutide, an incretin-based therapy, has also demonstrated therapeutic efficacy in MASH, including improvements in steatohepatitis and fibrosis-related endpoints [6]. Nevertheless, despite these advances, there remains a substantial unmet need for additional effective therapies targeting MASH.

Bile acid signaling has emerged as a key regulator of metabolic and inflammatory pathways through the gut—liver axis and a promising therapeutic target for MASLD/MASH [7—9]. Primary bile acids are synthesized from cholesterol in the liver, conjugated, and secreted into the intestine, where they facilitate dietary lipid absorption. The classical bile acid synthesis pathway is initiated by cholesterol 7α-hydroxylase (CYP7A1) and predominantly generates cholic acid (CA), whereas the alternative pathway is initiated by sterol 27-hydroxylase (CYP27A1) and favors the production of chenodeoxycholic acid (CDCA) [10]. In rodents, most CDCA is subsequently converted into muricholic acid (MCA) species by CYP2C70, an enzyme that is absent in humans, resulting in marked species-specific differences in bile acid composition [11]. In the intestine, primary bile acids are deconjugated by microbial bile salt hydrolase (BSH) and can subsequently be converted into secondary bile acids [12]. Previous clinical studies have shown that fecal BSH gene abundance is positively associated with liver disease severity, accompanied by alterations in the gut microbiome and bile acid profiles, suggesting that BSH-related microbial bile acid metabolism may serve as a biomarker of MASLD/MASH progression [13—15]. More recently, direct measurement of fecal BSH activity demonstrated increased activity in patients with MASLD and advanced liver fibrosis, further supporting microbial BSH as a potential therapeutic target for MASLD/MASH [16]. Experimental evidence also indicates that modulation of BSH activity in a single bacterial strain can markedly alter host bile acid composition and systemic metabolic homeostasis [17]. Notably, inhibition of microbial BSH improves gut barrier function and attenuates liver injury, underscoring its therapeutic potential in liver disease [18].

In this study, we assessed the therapeutic efficacy of GR-7, a bile salt hydrolase (BSH) inhibitor, in mouse models of MASH. GR-7 was previously described as an α-fluoromethyl ketone—based inhibitor that covalently targets the catalytic cysteine residue of BSH [18].

2. MATERIALS AND METHODS

2.1. Metabolic dysfunction—associated steatohepatitis (MASH) mouse model

All animal experiments were performed in at least two independent batches. Male C57BL/6 *Foz/Foz* mice carrying a homozygous loss-of-function mutation in the *Alms1* gene were used as described by us [19]. These mice exhibit hyperphagia, and when fed a Western diet (WD), develop pronounced obesity, insulin resistance, dyslipidemia, hepatic steatosis, steatohepatitis, and fibrosis compared with wild-type mice. This model recapitulates several key metabolomic and histopathological features of human MASLD/MASH [19,20]. At 6 weeks of age, mice were fed a WD for 24 weeks to induce MASH. The WD provided 40% kcal from fat (milk fat, 12% saturated) and 0.2% cholesterol and was enriched in fructose (AIN-76A Western Diet 5342, Catalog #TD.200289, Envigo). The bile salt hydrolase (BSH) inhibitor GR-7 was incorporated into the diet by the manufacturer at concentrations (weight of drug/weight of diet (% w/w)) of 0.034% (low dose) or 0.1% (high dose), and all diets were irradiated. Mice were randomly assigned to six groups: chow diet ($n = 7$), WD alone ($n = 12$), WD + low-dose GR-7 early intervention ($n = 10$), WD + high-dose GR-7 early intervention ($n = 12$), WD + low-dose GR-7 late intervention ($n = 6$), and WD + high-dose GR-7 late intervention ($n = 12$) (Figure 1). In the early intervention model, GR-7 was introduced after 3 weeks of WD feeding, whereas in the late intervention, treatment began after 12 weeks of WD feeding. Chow- and WD-fed animals served as shared controls for both intervention models. One mouse in the WD group died between weeks 6 and 7, two mice in the WD plus low-dose GR-7 early-intervention group died between weeks 21 and 23, and three mice in the WD plus high-dose GR-7 late-intervention group died between weeks 2 and 5 prior to initiation of GR-7 treatment and while receiving WD alone. Tissue samples were not collected from these six mice, and the causes of death could not be definitively determined. However, the mortality pattern was not dose- dependent, and four of the six deaths occurred while the mice were receiving WD alone, without GR-7 treatment. Mouse body weight and food intake were recorded weekly. Food intake was calculated on a per-mouse, per-day basis from cage-level consumption. All mice were euthanized at week 24 following an 8-hour fast.

2.2. One-week GR-7 treatment study to assess food intake and body weight gain (dietary administration)

Wild-type male C57BL/6 mice (6 weeks of age) were obtained from Charles River Laboratories and fed a WD for 3 weeks. Mice were then randomized into two groups and treated for an additional 1 week with either WD alone ($n = 10$) or WD supplemented with high-dose GR-7 (0.1% w/w; $n = 10$). Food intake and body weight were monitored throughout the treatment period, and body weight gain was calculated. Food intake was calculated on a per-mouse, per-day basis from cage-level consumption.

2.3. One-week GR-7 treatment study to assess food intake and body weight gain (oral gavage)

Wild-type male C57BL/6 mice (6 weeks of age) were obtained from Charles River Laboratories and fed a WD for 3 weeks. Mice were then maintained on WD and administered either PBS (100 μL; $n = 9$) or GR-7 (77 mg/kg in 100 μL PBS; $n = 9$) once daily for 1 week by oral gavage. The GR-7 dose was matched to the high-dose regimen used during late intervention based on average food intake. Food intake and body weight were recorded daily, and body weight gain was calculated over the treatment period. Food intake was calculated on a per-mouse, per-day basis from cage-level consumption.

2.4. Animal housing and ethics

Mice were housed under standard conditions with a 12 h light/12 h dark cycle, controlled temperature and humidity, and ad libitum access to food and water. All animal procedures were approved by the Institutional Animal Care and Use Committee at the University of California, San Diego (protocol number S09042) and conducted in accordance with institutional and ARRIVE guidelines.

2.5. RNA extraction and quantitative real-time PCR

Total RNA was extracted from intestinal tissues using TRIzol reagent (Invitrogen) according to the manufacturer's instructions. Genomic DNA contamination was removed using the DNA-free™ DNA Removal Kit (Ambion), and complementary DNA (cDNA) was synthesized using the High-Capacity cDNA Reverse Transcription Kit (Applied Biosystems). Primer sequences for mouse genes were originally obtained from the NIH qPrimerDepot database. Gene expression was quantified using SYBR Green chemistry (Bio-Rad Laboratories) on an ABI StepOnePlus Real-Time PCR System. Relative mRNA expression in the ileum was calculated using the $2^{-\Delta\Delta Ct}$ method and normalized to *Gapdh* as the

 Published by Elsevier GmbH. This is an open access article under the CC BY license (http://creativecommons.org/licenses/by/4.0/).

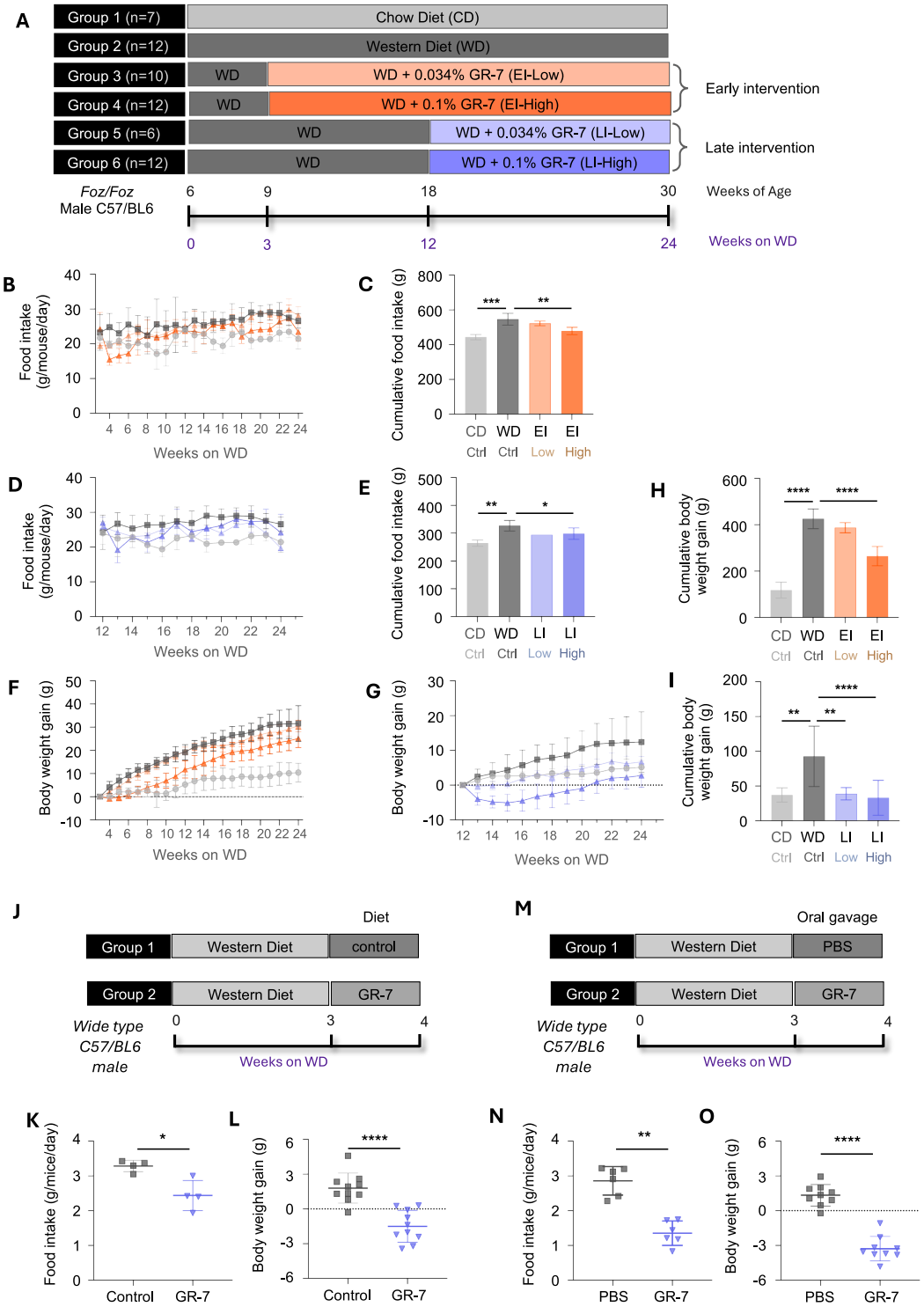


Figure 1: The BSH inhibitor GR-7 reduces food intake and body weight gain in western diet–fed mice. **A**, Experimental design. Male C57BL/6 *Foz/Foz* mice were fed chow diet (CD) or western diet (WD). GR-7 was administered either as early intervention (EI) starting at week 3 of WD feeding or as late intervention (LI) starting at week 12, at low (0.034%) or high (0.1%) dietary doses. Group sizes are indicated. **B**, Longitudinal food intake during early intervention. **C**, Cumulative food intake during early intervention. **D**, Longitudinal food intake during late intervention. **E**, Cumulative food intake during late intervention. **F**, Longitudinal body weight gain during early intervention. **G**, Longitudinal body weight gain during late intervention. **H**, Cumulative body weight gain during early intervention. **I**, Cumulative body weight gain during late intervention. **J**, Short-term dietary GR-7 intervention schematic in WD-fed wild-type mice. **K**, Daily food intake following short-term dietary GR-7 treatment. **L**, Body weight gain during short-term dietary GR-7 treatment. **M**, Oral gavage intervention schematic in WD-fed wild-type mice receiving PBS or GR-7. **N**, Daily food intake following oral gavage of PBS or GR-7. **O**, Body weight gain following oral gavage of PBS or GR-7. Data are shown as mean ± SD. Each symbol represents one mouse/one cage. Statistical significance was determined by one-way ANOVA with Bonferroni's multiple-comparisons test. For comparisons between two groups, Mann–Whitney U test was used. $^{*}P < 0.05$; $^{**}P < 0.01$; $^{***}P < 0.001$; $^{****}P < 0.0001$.

 Published by Elsevier GmbH. This is an open access article under the CC BY license (http://creativecommons.org/licenses/by/4.0/).

internal control. The primer sequences were as follows: mouse *Gapdh* (forward: 5′-TTGATGGCAACAATCTCCAC-3′; reverse: 5′-CGTC CCGTAGACAAAATGGT-3′); mouse *Nr1h4* (FXR) (forward: 5′-GGCAGA ATCTGGATTTGGAATCG-3′; reverse: 5′-GCCCAGGTTGGAATAGTAAGA CG-3′); mouse *Fgf15* (forward: 5′-ATGGCGAGAAAGTGGAACGG-3′; reverse: 5′-GGACCAGCGGAGTACAGGT-3′); mouse *Slc51b* (OSTβ) (forward: 5′-AGAGAAAGCTGCAGCCAATG-3′; reverse: 5′-CCAGGACCA GGATGGAATAA-3′); and mouse *Fabp6* (IBABP) (forward: 5′-CTTC CAGGAGACGTGATTGAAA-3′; reverse: 5′-AACTTGTTGCTCATAATGTT GCC-3′).

2.6. Histological staining and image analysis

Formalin-fixed tissue samples were embedded in paraffin (Paraplast Plus, McCormick), sectioned at 4 μm, and stained with hematoxylin and eosin (H&E; Surgipath) or 0.1% picrosirius red (PSR; Color Index 35780, 365548; Sigma—Aldrich). PSR-stained fibrotic area was quantified using ImageJ software (version 1.53k; Java 13.0.6). For detection of neutral lipid accumulation, liver tissues were embedded in OCT compound, sectioned at 10 μm on a cryostat, and stained with Oil Red O (Sigma—Aldrich). Quantification of Oil Red O—positive area was performed using ImageJ.

2.7. Biochemical analysis

Plasma alanine aminotransferase (ALT) levels were measured using the ALT (SGPT) Kinetic Liquid Assay (Teco Diagnostics). Hepatic triglyceride and cholesterol concentrations were quantified using Triglyceride Liquid Reagents and Cholesterol Liquid Reagents kits, respectively (Pointe Scientific). Plasma lipopolysaccharide (LPS) levels were assessed by enzyme-linked immunosorbent assay (ELISA; Lifeome Biolabs).

Liver hydroxyproline content was quantified using a chloramine T-Ehrlich colorimetric assay. Approximately 100 mg of liver tissue was homogenized in 1.5 mL of 6 N HCl and hydrolyzed at 110 °C for 16—18 h. Hydrolysates were filtered, plated in triplicate, dried, and reconstituted in water. A 0—200 μg/mL standard curve was prepared using trans-4-hydroxy-L-proline (Sigma—Aldrich). Samples and standards were reacted with chloramine T (C9887; Sigma—Aldrich) and Ehrlich's perchloric acid solution (AC168760250; Thermo Fisher Scientific). Absorbance was measured at 558 nm using a VersaMax microplate reader (Molecular Devices LLC, Sunnyvale, CA). Hydroxyproline content was calculated from the standard curve and normalized to liver tissue weight.

2.8. Bile acid extraction and quantification

Cecum contents were weighed and homogenized in water with metal beads, followed by protein precipitation with acetonitrile. Supernatants were diluted with a mixture of internal standard solution containing 14 deuterium-labeled bile acids and acetonitrile prior to analysis. Bile acids were quantified by UPLC-MS/MS using an Agilent 1290 UHPLC coupled to an Agilent 6495B triple quadrupole mass spectrometer operated in multiple-reaction monitoring mode with negative-ion detection (Creative Proteomics, Inc., Shirley, NY). Separation was performed on a Waters C18 column (2.1 × 150 mm, 1.7 μm) with a binary solvent gradient of 0.01% formic acid in water and acetonitrile. Calibration curves were constructed from serially diluted bile acid standards (0.00002—10 μM), and sample concentrations were determined using analyte-to-internal standard peak area ratios.

2.9. RNA-seq and data analysis

Total RNA was extracted from liver tissues using the QIAGEN RNeasy Mini Tissue Extraction Kit, with genomic DNA removed via DNase treatment. RNA quality and quantity were assessed prior to library preparation. Libraries were constructed from 100 ng of RNA per sample using the QIAGEN QIAseq UPXome RNA Library Kit with QIAseq FastSelect rRNA depletion and N6-T reverse transcription primers. After reverse transcription, 12 samples were pooled per batch and amplified for 15 PCR cycles. Sequencing was performed on the MGI DNBSEQ-T7 platform. Raw reads were quality-checked, trimmed, and aligned to the reference genome using standard RNA-seq pipelines (Gnomix, South Australia, Australia). Gene-level expression data were imported into R (v4.5.2), merged across samples by gene identifier, and missing values were set to zero. Genes with positive expression in at least one-third of samples were retained to reduce low-abundance noise, yielding 15,519 high-quality genes. Expression consistency across samples was assessed using log10-transformed TPM distributions and quality control metrics. Differential expression analysis was performed on protein-coding exon count matrices using DESeq2 after low-expression filtering (CPM >1 in at least three samples), followed by size-factor normalization and variance-stabilizing transformation. Differential expression was modeled using a negative binomial generalized linear model with experimental condition as the design factor, and significant genes were defined by adjusted $P < 0.05$ and contrast-specific fold-change thresholds. KEGG pathway enrichment analysis was conducted on significantly upregulated and downregulated genes (adjusted $P < 0.1$, |fold change| ≥ 1.2), with enriched pathways ranked by adjusted P value and fold enrichment and visualized using dot plots. RNA-seq data generated in this study have been deposited in the GEO database under accession number GSE342274.

2.10. Immune cell isolation, staining, and mass cytometry (CyTOF) analysis

Single-cell suspensions were prepared from freshly isolated mouse livers by mechanical dissociation, red blood cell lysis, and Percoll density-gradient centrifugation. Purified cells were washed, resuspended in complete medium, and counted prior to analysis. For mass cytometry, cells were stained with a panel of metal-conjugated antibodies. Briefly, cells were first labeled with cisplatin (Cell-ID Cisplatin, Fluidigm) for live/dead discrimination, followed by sample barcoding (Cell-ID 20-Plex Pd Barcoding kit, PN PRD023, Fluidigm), and staining of surface markers. Cells were then fixed, permeabilized, and stained for intracellular cytokines and cytoplasmic proteins. After final fixation, DNA was labeled with an intercalator (Cell-ID Intercalator, Fluidigm) prior to acquisition on a CyTOF mass cytometer. The antibody panel included markers defining major immune lineages, activation and exhaustion states, and effector cytokines (see Supplemental Table1 for details). Samples were resuspended in Cell Acquisition Solution supplemented with EQ calibration beads and acquired on a CyTOF mass cytometer (Fluidigm), with approximately 300,000—800,000 events collected per sample depending on cell yield. Data were normalized using EQ bead-based signal correction, and quality control steps included removal of beads, doublets, debris, and dead cells based on cisplatin and DNA intercalator signals. Immune populations were defined by sequential gating of $CD45^+$ leukocytes and lineage-specific markers using Cytobank and downstream computational analysis workflows (Standard BioTools, Ontario, Canada).

2.11. Statistical analysis

Results are expressed as mean ± standard deviation (SD). At least two technical replicates were performed in each of the groups. Significance was evaluated using One-way analysis of variance (ANOVA)

 Published by Elsevier GmbH. This is an open access article under the CC BY license (http://creativecommons.org/licenses/by/4.0/).

followed by Bonferroni's multiple comparisons test for experiments involving three or more groups. The mean of each column was compared to the mean of western diet-fed control mice. Statistical comparison between two groups was conducted using a two-tailed unpaired Mann—Whitney U test. A P value < 0.05 was considered to be statistically significant. All statistical analyses were performed using GraphPad Prism v10.3.0.

3. RESULTS

3.1. GR-7 reduces food intake and attenuates body weight gain in MASH mouse models

To evaluate the efficacy of the BSH inhibitor GR-7 in MASH, we used an established diet-induced MASH model by feeding male *Alms1*-deficient C57BL/6 (*Foz/Foz*) mice a Western diet (WD) for 24 weeks (Figure 1A) [19]. Chow diet (CD) fed mice served as normal controls. To assess early intervention, mice were administered either a low dose (0.034% weight of drug/weight of diet (w/w)) or a high dose (0.1% w/w) of GR-7 starting after 3 weeks of WD feeding and continued until week 24. To evaluate late intervention, separate cohorts received the same low or high doses of GR-7 beginning after 12 weeks of WD feeding and continued until week 24. Food intake and body weight were monitored weekly throughout the study.

Compared with WD-fed controls, mice receiving the high dose of GR-7 exhibited a significant reduction in food intake during both early and late intervention phases, whereas the low dose of GR-7 showed a nonsignificant downward trend (Figure 1B—E). High-dose GR-7 significantly attenuated WD-induced weight gain in both early and late intervention settings, while the low dose significantly reduced body weight gain only during the late intervention phase (Figure 1F—I).

Because *Foz/Foz* mice exhibit hyperphagia, we next sought to determine whether GR-7 exerted similar effects in wild-type mice. A short-term experiment was conducted in male wild-type C57BL/6 mice, which were fed WD for 3 weeks followed by one week of either control diet or WD supplemented with 0.1% GR-7 (Figure 1J). One week of high-dose GR-7 supplementation significantly reduced both food intake and body weight gain compared with controls (Figure 1K-L).

To further exclude the possibility that reduced food intake resulted from altered diet palatability or odor, GR-7 administration was switched from dietary supplementation to oral gavage (Figure 1M). Consistently, mice receiving GR-7 by gavage displayed significantly reduced food intake and body weight gain compared with PBS-treated controls (Figure 1N-O).

Collectively, these results demonstrate that GR-7 reduces food intake and attenuates body weight gain in both WD-fed *Foz/Foz* and wild-type mice, with greater efficacy observed at higher dosage, supporting a dose-dependent metabolic effect independent of dietary palatability.

3.2. Early intervention with GR-7 attenuates hepatic cholesterol accumulation and fibrosis

To evaluate the efficacy of early intervention with GR-7, a comprehensive assessment of hepatic metabolic and histological parameters was performed. Compared with chow-fed controls, WD feeding resulted in significant increases in liver weight and liver-to-body weight ratio (Figure 2A—B; all $P < 0.0001$), accompanied by marked elevations in hepatic triglyceride and cholesterol levels and enhanced Oil Red O staining, indicative of substantial hepatic lipid accumulation (Figure 2C—E, J; all $P < 0.0001$). Early intervention with high-dose GR-7 significantly reduced liver weight, liver-to-body weight ratio, and total hepatic cholesterol compared with WD-fed mice (Figure 2A, B, and D; all $P < 0.01$). Early intervention resulted in lower total hepatic triglycerides and Oil Red O staining, although this was not statistically significant (Figure 2C, E, and J).

Plasma alanine aminotransferase (ALT) and lipopolysaccharide (LPS) levels were not significantly altered by WD feeding (Figure 2F—G), likely reflecting elevated baseline values in obese chow-fed *Foz/Foz* mice. In contrast, WD feeding markedly increased hepatic hydroxyproline content and Picro-Sirius Red—positive staining, indicating enhanced liver fibrosis (Figure 2H—J). Notably, administration of GR-7 during early intervention significantly attenuated these fibrosis indices, even at a low dose. Early intervention lowered plasma ALT and LPS levels, although this was not statistically significant (Figure 2F—G).

Collectively, these findings demonstrate that early intervention with GR-7 confers protection against MASH development, characterized by lower lipid accumulation and robust anti-fibrotic effects even at a low dose.

3.3. Late intervention with GR-7 attenuates hepatic lipid accumulation and inflammation

To evaluate the therapeutic efficacy of late intervention with GR-7 in established MASH, hepatic metabolic and histological parameters were assessed. Compared with WD—fed controls, only high-dose GR-7 treatment significantly reduced liver weight, liver-to-body weight ratio, and total hepatic triglyceride and cholesterol levels, findings that were consistent with quantitative Oil Red O staining (Figure 2A—E, J; all $P < 0.05$). These results indicate that high-dose GR-7 effectively attenuates hepatic lipid accumulation when administered after disease establishment. In addition, therapeutic high-dose GR-7 significantly decreased plasma ALT and LPS levels, suggesting reduced hepatic inflammation and improved intestinal barrier integrity (Figure 2F—G; all $P < 0.05$). Hepatic fibrosis was lower following late intervention, although this was not significantly different, indicating that the anti-fibrotic effects of GR-7 may require longer treatment (Figure 2H—J).

Collectively, these findings demonstrate that late intervention GR-7 administration reverses hepatic steatosis and inflammation and improves gut barrier function in a dose-dependent manner.

3.4. Pharmacological inhibition of BSH activity modulates cecal bile acid profiles

To assess the *in vivo* efficacy of the BSH inhibitor GR-7, targeted bile acid profiling was performed in cecal contents. Unconjugated bile acids constituted more than 90% of the total bile acid in the cecum, consistent with efficient ileal reabsorption of conjugated bile acids and extensive bacterial BSH activity in the cecum. Compared with chow-fed controls, WD feeding markedly increased total primary unconjugated bile acids (Figure 3A, $P < 0.0001$), whereas total primary conjugated bile acids were not significantly altered (Figure 3B). This diet-induced enhancement of bile acid deconjugation was significantly reversed by high-dose GR-7 treatment in both early and late intervention settings, with pronounced reductions in α-muricholic acid (α-MCA) and β-muricholic acid (β-MCA) (Figure 3A, all $P < 0.05$), consistent with effective inhibition of bacterial BSH activity *in vivo*. There was a trend toward lower levels of cholic acid (CA) and chenodeoxycholic acid (CDCA) with high-dose GR-7 treatment. WD feeding also significantly increased total secondary bile acids, including both conjugated and unconjugated species (Figure 3C—D, all $P < 0.001$), reflecting enhanced microbial bile acid transformation. Administration of GR-7 effectively suppressed secondary bile acid accumulation in both early and late-stage interventions (Figure 3C—D, all $P < 0.05$). Notably, low-dose GR-7 was sufficient to reduce total secondary bile acids,

 Published by Elsevier GmbH. This is an open access article under the CC BY license (http://creativecommons.org/licenses/by/4.0/).

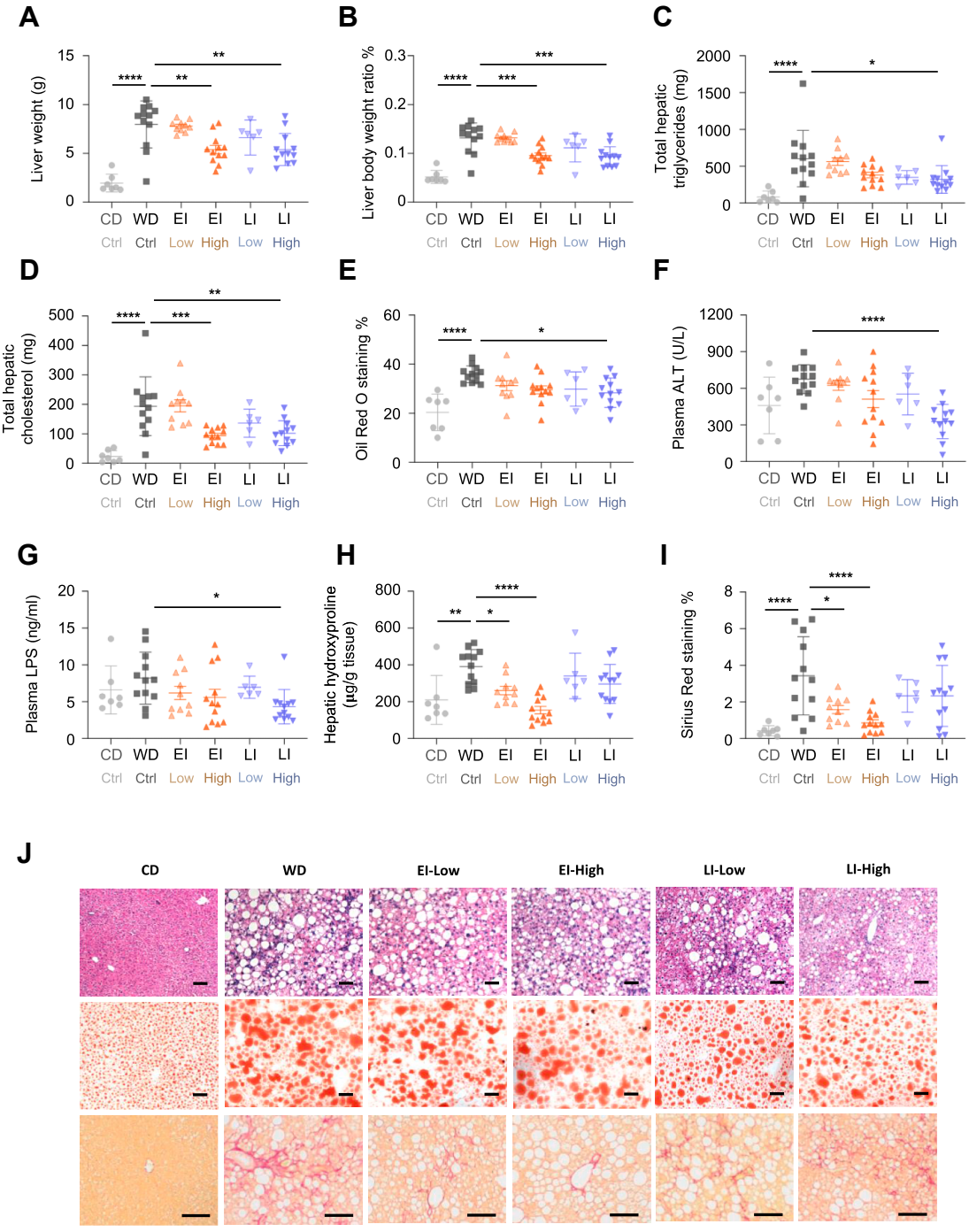


Figure 2: GR-7 ameliorates hepatic steatosis, inflammation, and fibrosis in western diet–fed mice. A, Liver weight. **B**, Liver-to-body weight ratio. **C**, Total hepatic triglyceride content. **D**, Total hepatic cholesterol content. **E**, Quantification of Oil Red O–positive area. **F**, Plasma alanine aminotransferase (ALT) levels. **G**, Plasma lipopolysaccharide (LPS) levels. **H**, Hepatic hydroxyproline content. **I**, Quantification of Picro-Sirius Red–positive area. **J**, Representative histological images of liver sections from chow diet (CD), western diet (WD), early-intervention low-dose (EI-Low), early-intervention high-dose (EI-High), late-intervention low-dose (LI-Low), and late-intervention high-dose (LI-High) groups. Top row: H&E staining; middle row: Oil Red O staining; bottom row: Picro-Sirius Red staining. Scale bars, 50 μm. Data are shown as mean ± SD. Each symbol represents one mouse. Statistical significance was determined by one-way ANOVA with Bonferroni's multiple-comparisons test. $*P < 0.05$; $**P < 0.01$; $***P < 0.001$; $****P < 0.0001$.

whereas high-dose treatment exerted a more pronounced effect on total secondary unconjugated bile acids (Figure 3C), further supporting dose-dependent suppression of microbial bile acid deconjugation and downstream secondary bile acid formation. Collectively, these findings demonstrate that GR-7 robustly changes cecal bile acids through inhibition of bacterial BSH activity *in vivo*.

 Published by Elsevier GmbH. This is an open access article under the CC BY license (http://creativecommons.org/licenses/by/4.0/).

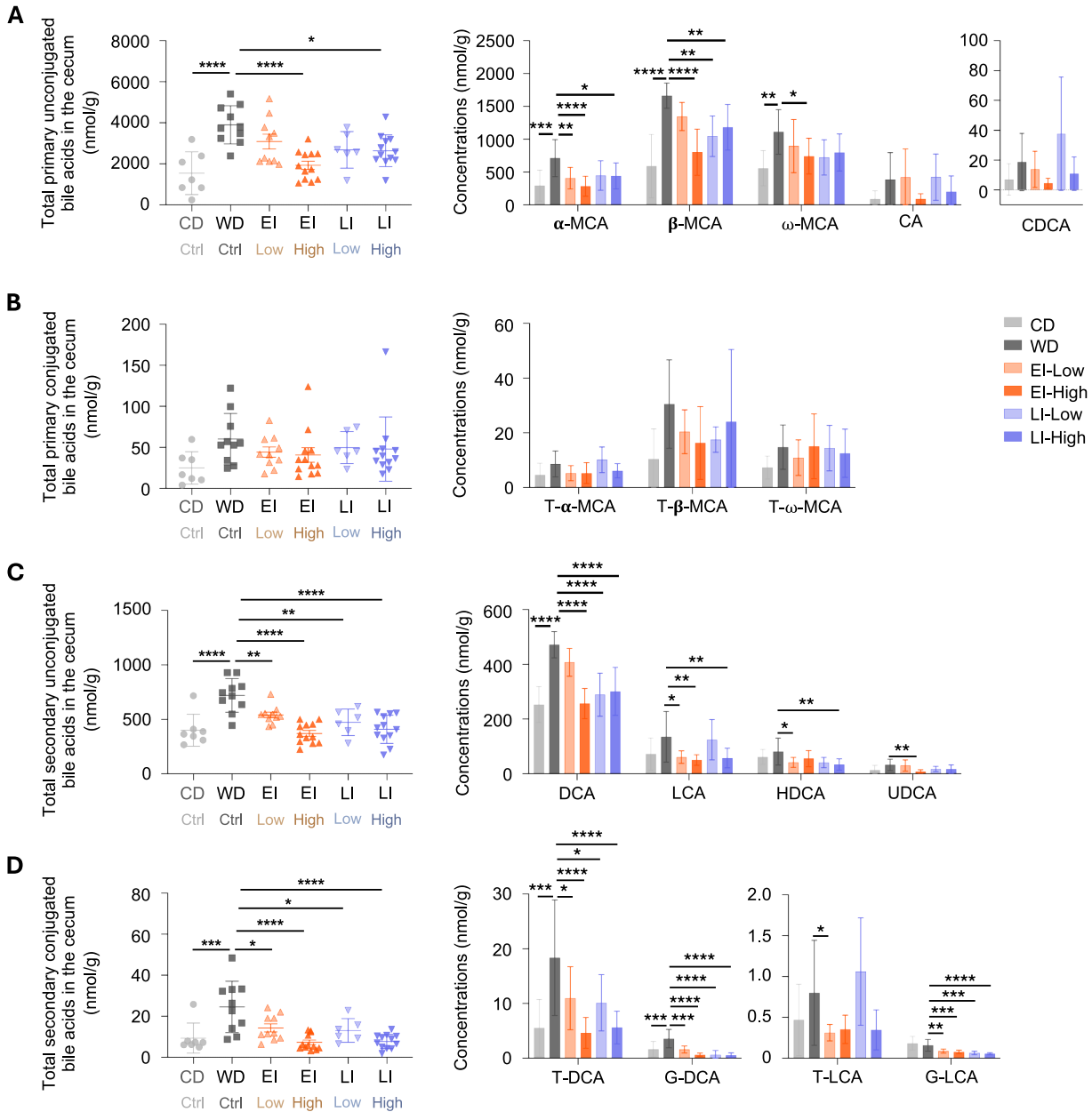


Figure 3: GR-7 changes cecal bile acid composition. A, Total primary unconjugated bile acids in cecal contents (left) and concentrations of representative individual primary unconjugated bile acid species, including α-muricholic acid (α-MCA), β-muricholic acid (β-MCA), ω-muricholic acid (ω-MCA), cholic acid (CA), and chenodeoxycholic acid (CDCA) (right). **B**, Total primary conjugated bile acids in cecal contents (left) and concentrations of representative individual taurine-conjugated primary bile acids, including tauro-α-muricholic acid (T-α-MCA), tauro-β-muricholic acid (T-β-MCA), and tauro-ω-muricholic acid (T-ω-MCA) (right). **C**, Total secondary unconjugated bile acids in cecal contents (left) and concentrations of representative individual secondary unconjugated bile acid species, including deoxycholic acid (DCA), lithocholic acid (LCA), hyodeoxycholic acid (HDCA), and ursodeoxycholic acid (UDCA) (right). **D**, Total secondary conjugated bile acids in cecal contents (left) and concentrations of representative individual taurine- or glycine-conjugated secondary bile acids, including tauro-deoxycholic acid (T-DCA), glyco-deoxycholic acid (G-DCA), tauro-lithocholic acid (T-LCA), and glyco-lithocholic acid (G-LCA) (right). Cecal bile acids were quantified by targeted bile acid profiling. Data are shown as mean ± SD. Each symbol represents one mouse. Statistical significance was determined by one-way ANOVA with Bonferroni's multiple-comparisons test. $*P < 0.05$; $**P < 0.01$; $***P < 0.001$; $****P < 0.0001$.

3.5. BSH inhibition reshapes hepatic gene expression in MASH during late intervention

To further elucidate the molecular mechanisms underlying the therapeutic effects of BSH inhibition, RNA sequencing was performed on liver tissues. Because late intervention with high-dose GR-7 was most effective in suppressing MASH, subsequent transcriptomic analyses focused on comparisons between WD-fed mice and WD-fed mice receiving late intervention with high-dose GR-7. Substantial transcriptional reprogramming was observed in the liver following high-dose GR-7 treatment, with clear separation from WD-fed controls (Figure 4A). KEGG pathway enrichment analysis revealed coordinated regulation of multiple metabolic and inflammatory pathways (Figure 4B). Specifically, GR-7 administration significantly upregulated bile acid—related pathways, including steroid hormone biosynthesis, cholesterol metabolism, and bile secretion. In parallel, lipid metabolic pathways such as linoleic acid metabolism and arachidonic acid

 Published by Elsevier GmbH. This is an open access article under the CC BY license (http://creativecommons.org/licenses/by/4.0/).

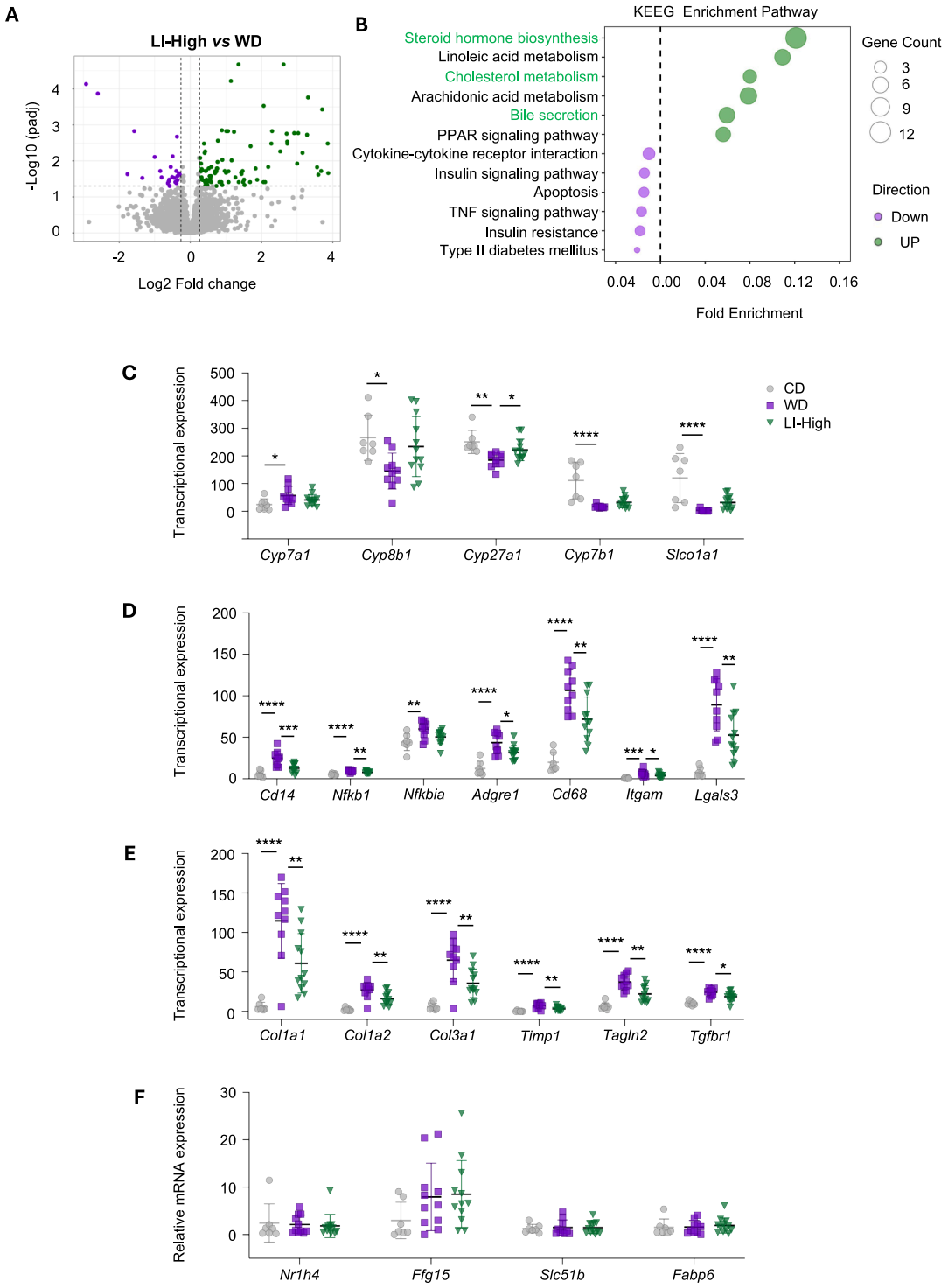


Figure 4: Late intervention with high-dose GR-7 reprograms hepatic transcriptome toward alternative bile acid synthesis and suppresses inflammatory and fibrotic signaling. A, Volcano plot showing differentially expressed hepatic genes in the LI-High group compared with WD controls. Dotted vertical lines indicate $\log_2$ fold-change thresholds, and the horizontal dashed line indicates the adjusted *P*-value cutoff. Upregulated and downregulated genes are highlighted. **B,** KEGG pathway enrichment analysis of differentially expressed genes in livers from LI-High versus WD groups. Bubble size indicates gene count, and color denotes the direction of regulation (upregulated or downregulated). Differentially expressed genes were defined using an adjusted *P*-value cutoff of 0.1 and an absolute fold-change threshold of 1.2. **C**, Hepatic expression of bile acid synthesis and transport—related genes, including *Cyp7a1*, *Cyp8b1*, *Cyp27a1*, *Cyp7b1*, and *Slco1a1*. **D**, Hepatic expression of inflammation- and immune-related genes, including *Cd14*, *Nfkb1*, *Nfkbia*, *Adgre1*, *Cd68*, *Itgam*, and *Lgals3*. **E**, Hepatic expression of fibrosis-related genes, including *Col1a1*, *Col1a2*, *Col3a1*, *Timp1*, *Tagln2*, and *Tgfbr1*. **F**, Relative ileal mRNA expression of FXR (*Nr1h4*) and its targeted genes *Fgf15*, *Slc51b* (OSTβ), and *Fabp6* (IBABP), as determined by quantitative reverse transcription PCR (RT-qPCR). **C-E,** Gene expression levels were quantified by RNA sequencing and are shown as normalized transcript abundance. CD: chow diet; WD: Western diet; LI-High: Late intervention with high dose. Data are shown as mean ± SD. Each symbol represents one mouse. Statistical significance was assessed using the one-way ANOVA with Bonferroni's multiple comparisons test. $^{*}P < 0.05$; $^{**}P < 0.01$; $^{***}P < 0.001$; $^{****}P < 0.0001$.

 Published by Elsevier GmbH. This is an open access article under the CC BY license (http://creativecommons.org/licenses/by/4.0/).
www.molecularmetabolism.com

metabolism were also significantly modulated. In contrast, pathways associated with insulin resistance and inflammation—including cytokine–cytokine receptor interaction and TNF signaling—were markedly downregulated. These transcriptional changes were consistent with the observed phenotypic improvements in hepatic steatosis and inflammation following high-dose therapeutic BSH inhibition.

To further dissect bile acid–specific regulatory mechanisms, we examined the expression of genes involved in hepatic bile acid synthesis (Figure 4C). Compared with chow-fed controls, WD feeding significantly increased expression of *Cyp7a1*, which encodes the rate-limiting enzyme of the classical bile acid synthesis pathway; this induction was not significantly altered by BSH inhibitor treatment. In contrast, WD feeding suppressed *Cyp27a1*, which encodes a key enzyme in the alternative bile acid synthesis pathway, and this suppression was robustly reversed by GR-7, indicating a shift toward enhanced alternative bile acid synthesis. Similarly, genes encoding downstream enzymes involved in bile acid synthesis, including *Cyp8b1* and *Cyp7b1*, were downregulated under WD conditions and showed a trend toward restoration following BSH inhibitor treatment, although these changes did not reach statistical significance. In addition to bile acid synthesis, hepatic bile acid transport was also affected. Among bile acid transporters, *Slco1a1* was significantly downregulated by WD feeding but exhibited a trend toward restoration in the BSH inhibitor–treated group, suggesting enhanced hepatocellular uptake of portal bile acids in response to intestinal bile acid remodeling.

Analysis of inflammatory gene expression further supported an anti-inflammatory effect of BSH inhibition. Multiple genes upregulated by WD feeding were significantly suppressed by GR-7 treatment, including *Cd14* and *Nfkb1*, while *Nfkbia* showed a trend toward reduction (Figure 4D). These genes are associated with gut barrier dysfunction and inflammatory signaling. Moreover, macrophage- and Kupffer cell–associated markers such as *Adgre1*, *Cd68*, *Itgam*, and *Lgals3* were also markedly reduced, indicating attenuation of hepatic innate immune activation (Figure 4D). Although late-stage intervention with high-dose GR-7 treatment did not result in statistically significant improvement in histological fibrosis, transcriptomic analysis revealed significant downregulation of several fibrosis-associated genes, including *Col1a1, Col1a2, Col3a1, Timp1, Tagln2, and Tgfbr1* (Figure 4E). In addition, quantitative PCR analysis showed no significant differences in ileal mRNA expression of FXR (*Nr1h4*) or the FXR target genes *Fgf15*, *Slc51b* (OSTβ), and *Fabp6* (IBABP) following high-dose GR-7 treatment (Figure 4F). These changes indicate that BSH inhibition may exert early anti-fibrotic effects at the transcriptional level that precede detectable histological improvement.

Taken together, these transcriptomic data demonstrate that late therapeutic intervention with high-dose BSH inhibitor induces broad transcriptional reprogramming in the liver, characterized by enhanced bile acid metabolic remodeling, suppression of inflammatory signaling, and attenuation of fibrosis-related gene expression, thereby contributing to the overall improvement of MASH pathology.

3.6. CyTOF profiling reveals Western diet-induced immune remodeling and its modulation by late intervention with GR-7

To comprehensively characterize hepatic immune alterations induced by WD feeding and late intervention with GR-7, we performed high-dimensional mass cytometry (CyTOF) analysis on liver immune cells (Figure 5A). Unsupervised CyTOF analysis demonstrated that, compared with chow diet–fed mice, WD feeding profoundly remodeled the hepatic immune compartment. Specifically, WD-fed mice exhibited a significant reduction in T cells accompanied by an increase in B cells (Figure 5B). Overall CD4 T cells were significantly decreased, whereas regulatory CD4 T cells (Tregs) were increased (Figure 5C). At the functional level, CyTOF profiling further revealed significant suppression of IL-17A^{+} CD4 T cells and granzyme B^{+} CD8 T cells (Figure 5D). Collectively, these data indicate that western diet feeding drives the liver into an immunosuppressed yet dysregulated state, characterized by impaired adaptive immune effector functions and compensatory expansion of regulatory immune populations, rather than overt inflammatory activation.

CyTOF-based immune profiling further revealed that late intervention with high-dose GR-7 did not globally normalize hepatic immune cell distributions to chow-fed levels; instead, several immune populations were selectively altered compared with WD-fed mice. Notably, dendritic cells were significantly increased following late intervention with high-dose GR-7 treatment, indicating alterations in antigen-presenting cell compartments during late-stage intervention (Figure 5B). Among immune subpopulations, late intervention with high-dose treatment resulted in a significant reduction in Tregs compared with WD-fed mice. In parallel, CyTOF analysis demonstrated a significant increase in activated NK cells, together with an increase in M2 macrophages and CD11b^{+} F4/80^{hi} macrophages, indicating altered innate immune activation and macrophage polarization during late-stage intervention (Figure 5C). At the T cell cytokine level, late intervention with high-dose treatment significantly increased IL-2^{+} CD4 T cells and IL-4^{+} CD4 T cells, consistent with enhanced immunoregulatory and Th2-associated cytokine programs (Figure 5D). Taken together, these results demonstrate that late intervention with high-dose BSH inhibition does not fully restore hepatic immune composition to a chow-fed state, but instead selectively reshapes the immune microenvironment by recalibrating regulatory, innate, and cytokine-associated immune programs during established disease.

4. DISCUSSION

Here, we demonstrate that pharmacological inhibition of microbial BSH using the inhibitor GR-7 exerts stage- and dose-dependent therapeutic effects in a mouse model of MASH. GR-7 reduced food intake and body weight gain. Early intervention with GR-7 robustly suppressed hepatic fibrosis even at a low dose. Although early and late intervention reduced hepatic steatosis and injury, only late-stage administration of high-dose GR-7 exerted pronounced effects on hepatic steatosis, inflammation, and injury. However, fibrosis was not histologically reversed at this stage and was instead suppressed primarily at the transcriptional level. Collectively, these findings indicate that microbial BSH inhibition holds substantial therapeutic potential for MASH, with efficacy strongly influenced by both treatment timing and dosage.

We further validated the *in vivo* efficacy of GR-7 as a BSH inhibitor by profiling bile acid composition in the cecum, a major site of microbial bile acid metabolism. High-dose GR-7 significantly reduced total unconjugated primary bile acids in both early and late intervention settings, indicating that sufficient compound exposure is required to effectively engage the catalytic cysteine residue of BSH. Notably, the changes observed in the primary bile acid pool following GR-7 treatment were driven predominantly by MCA species, which constitute major primary bile acids in rodents. CDCA, a major primary bile acid in humans, also exhibited a reduction trend following GR-7 treatment, suggesting that the effects of GR-7 are not exclusively limited to rodent-specific bile acid species. This observation is

 Published by Elsevier GmbH. This is an open access article under the CC BY license (http://creativecommons.org/licenses/by/4.0/).

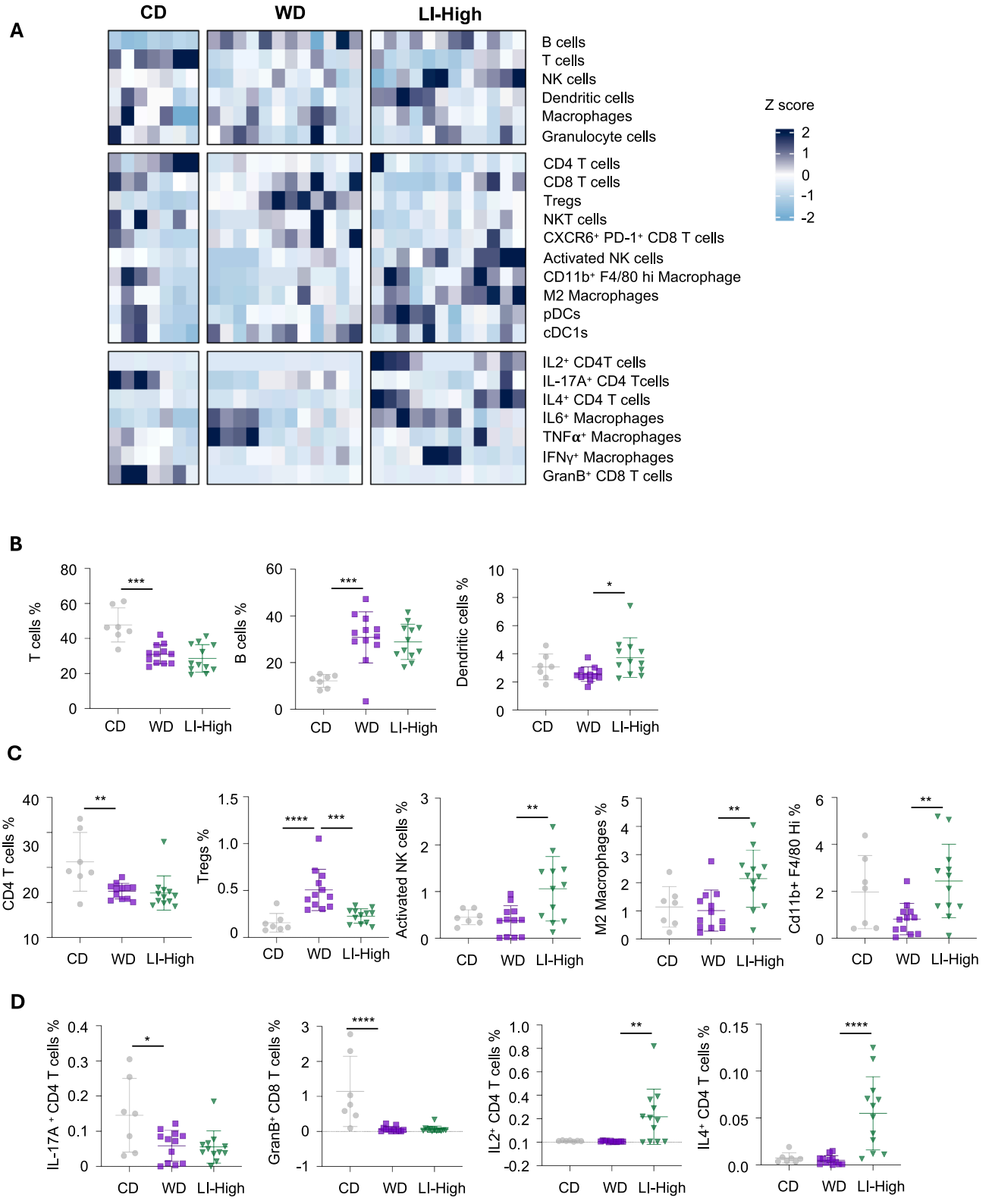


Figure 5: Late high-dose GR-7 remodels the hepatic immune landscape in western diet—fed mice. A, Heatmap summarizing CyTOF-based profiling of major hepatic immune cell populations, functional subpopulations, and cytokine-producing subsets in chow diet (CD), western diet (WD), and late-intervention high-dose GR-7 (LI-High) groups. Data are shown as Z scores for each immune population across individual mice. **B**, Percentages of total T cells, B cells, and dendritic cells among live hepatic immune cells. **C**, Percentages of immune cell subpopulations, including CD4 T cells, regulatory T cells (Tregs), activated NK cells, M2 macrophages, and CD11b^{+}F4/80^{hi} macrophages. **D**, Percentages of cytokine-producing immune cell subsets, including IL-17A^{+} CD4 T cells, Granzyme B^{+} CD8 T cells, IL-2^{+} CD4 T cells, and IL-4^{+} CD4 T cells. CyTOF analysis was performed on liver immune cells isolated at the study endpoint. Data are shown as mean ± SD. Each symbol represents one mouse. Statistical significance was determined by one-way ANOVA with Bonferroni's multiple comparisons test. *$P < 0.05$; **$P < 0.01$; ***$P < 0.001$; ****$P < 0.0001$.

 Published by Elsevier GmbH. This is an open access article under the CC BY license (http://creativecommons.org/licenses/by/4.0/).

consistent with previous reports demonstrating that BSH inhibitors exhibit broad-spectrum inhibitory activity across diverse bacterial strains and achieve effective target engagement *in vivo* [18]. Remarkably, GR-7 also reduced secondary bile acids, including both conjugated and unconjugated species, consistent with suppressed microbial bile acid deconjugation and downstream secondary bile acid formation. Because microbiome profiling was not performed, we cannot determine whether this effect resulted solely from direct inhibition of secondary bile acid—producing pathways or was also mediated by indirect changes in microbial composition. This represents a limitation of the present study. Nevertheless, the pronounced suppression of the highly hydrophobic bile acids deoxycholic acid (DCA) and lithocholic acid (LCA) is particularly relevant. Elevated levels of DCA and LCA have been implicated in hepatocyte injury, intestinal barrier dysfunction, and inflammatory signaling, and metabolomic profiling linked increased DCA and LCA levels with advanced liver fibrosis in patients [9,21]. These findings align with our observations, as GR-7 administration reduced cecal DCA and LCA levels and was associated with improved hepatic fibrosis. Mechanistically, these effects may be mediated, at least in part, through improved intestinal barrier integrity. Consistent with this hypothesis, prior studies have shown that BSH inhibition protects gut epithelial monolayers from damage induced by microbial-derived unconjugated bile acids via altered micelle formation *in vitro* [18]. In the present study, we observed similar protective effects *in vivo*, as evidenced by significantly reduced plasma LPS levels in the late intervention group receiving high-dose GR-7, with a similar downward trend observed in the early intervention group. Collectively, these findings indicate that high-dose GR-7 effectively reduces cecal unconjugated primary and secondary bile acids and confers hepatoprotective effects by attenuating hepatic inflammation, at least in part via restoration of gut barrier integrity and reduced microbial translocation.

Given that GR-7 is not intestinally absorbed [22], our findings indicate that inhibition of microbial BSH can nonetheless reprogram hepatic bile acid metabolism through altered gut—liver signaling. Hepatic RNA sequencing revealed enrichment of bile acid—related pathways, accompanied by increased expression of *Cyp27a1*, suggesting enhanced engagement of the alternative bile acid synthesis pathway. Consistent with our findings, recent studies have demonstrated that inhibition of microbial BSH activity can activate the alternative bile acid synthesis pathway and confer beneficial metabolic effects. For example, administration of theabrownin, a key bioactive component of Pu-erh tea, suppresses intestinal bacterial BSH activity, promotes alternative bile acid synthesis, and reduces cholesterol and lipid levels [23]. Other naturally occurring BSH inhibitors, including riboflavin and grape seed extracts, have also been reported to activate the alternative bile acid synthesis pathway, suggesting a conserved metabolic response to BSH inhibition [24,25]. In the present study, GR-7 preferentially increased Cyp27a1 expression without significantly altering Cyp7a1, indicating preferential modulation of the alternative rather than the classical bile acid synthesis pathway. This response may promote hepatic cholesterol utilization and the production of more hydrophilic bile acids, which could contribute to reduced intestinal cholesterol and lipid absorption, as previously reported [10]. Notably, enhanced activity of the alternative bile acid synthesis pathway has been proposed as a compensatory, protective response in advanced MASLD and fibrosis [10, 26], which may explain the greater therapeutic efficacy of GR-7 during late intervention compared with early intervention, highlighting disease stage—dependent metabolic plasticity as a key determinant of responsiveness to microbial BSH inhibition.

Considering that GR-7 directly suppresses microbial bile acid deconjugation, it may increase the availability of conjugated bile acids in the distal small intestine [10]. Because conjugated bile acids are predominantly reabsorbed in the terminal ileum, their transporter-mediated uptake may permit activation of ileal FXR signaling. However, in the present study, GR-7 treatment did not produce detectable changes in the ileal expression of FXR (*Nr1h4*) or its target genes *Fgf15*, *Slc51b*, and *Fabp6*. Species-specific differences in bile acid composition should nevertheless be considered when extrapolating these findings to humans. In humans, enhanced CYP27A1-mediated bile acid synthesis may favor the production of CDCA, a major primary bile acid and potent FXR agonist [27,28]. In rodents, by contrast, much of the CDCA is converted into MCA species, some of which, particularly tauro-β-muricholic acid, can antagonize FXR [11,29]. Therefore, FXR-mediated effects of BSH inhibition may be more pronounced in humans than in the present mouse model.

Furthermore, high-dose early intervention was associated with a significant reduction in food intake, which was also validated in wild-type mice. This effect may have partially contributed to the attenuation of MASLD progression, particularly with respect to hepatic lipid accumulation and body weight gain. Consistent with previous reports, mono-colonization with bile salt hydrolase—deficient *Bacteroides thetaiotaomicron* reduced body weight and food consumption through altered bile acid signaling rather than impaired nutrient absorption [17]. This metabolic reprogramming was accompanied by enhanced glycolysis and increased lipid uptake in ileal epithelial cells, supporting coordinated lipid utilization and energy homeostasis [17]. In addition, altered bile acid signaling may contribute to appetite regulation and reduced food intake through intestinal bile acid receptors, particularly the G protein—coupled bile acid receptor 1 (TGR5), and downstream glucagon-like peptide-1 secretion. However, whether this pathway contributes to the reduced food intake observed following GR-7 treatment remains to be determined [30—32].

Lastly, we investigated whether inhibition of microbial bile salt hydrolase (BSH) alters the hepatic immune landscape in MASH. Unbiased high-dimensional immune profiling by CyTOF revealed that western diet feeding induced profound remodeling of the hepatic immune compartment. However, GR-7 treatment did not globally restore these diet-induced immune alterations. Instead, it selectively reshaped the hepatic immune microenvironment by recalibrating regulatory, innate, and cytokine-associated immune programs during established disease. Notably, late intervention with high-dose GR-7 was associated with a shift in hepatic macrophage polarization toward an M2-like, immunoregulatory phenotype. This macrophage remodeling was accompanied by coordinated downregulation of inflammatory and macrophage-associated genes, including *Adgre1*, *Cd68*, *Itgam*, and *Lgals3*, which are closely linked to Kupffer cell activation. Together, these findings suggest that GR-7 promotes a more immunoregulatory hepatic environment rather than broadly suppressing immune responses, consistent with an improved inflammatory state during late-stage MASH. These immune changes are mechanistically consistent with GR-7—mediated reshaping of intestinal bile acid composition, particularly through reduction of hydrophobic and cytotoxic secondary bile acids such as DCA and LCA. Reduced plasma LPS would be expected to attenuate Toll-like receptor—mediated activation of hepatic macrophages, thereby limiting inflammatory Kupffer cell signaling and favoring a macrophage-dominant immunoregulatory state in established MASH.

In summary, our study demonstrates that pharmacological inhibition of microbial BSH by the non-absorbable compound GR-7 exerts stage- and dose-dependent therapeutic effects in a mouse model of

 Published by Elsevier GmbH. This is an open access article under the CC BY license (http://creativecommons.org/licenses/by/4.0/).

MASH. By suppressing microbial bile acid deconjugation, GR-7 reshapes the intestinal bile acid pool, reduces hydrophobic and cytotoxic secondary bile acids such as DCA and LCA, and improves intestinal barrier function, thereby limiting plasma LPSThese changes reprogram hepatic bile acid metabolism toward enhanced engagement of the alternative CYP27A1-mediated synthesis pathway, promote cholesterol utilization, and alleviate metabolic and inflammatory stress, particularly during late-stage disease. In addition, reduced food intake might have partially contributed to the metabolic benefits of GR-7. Given species-specific differences in bile acid composition, this pathway may have distinct translational consequences in humans, potentially favoring CDCA production and FXR-dependent signaling. Together, these findings establish microbial BSH inhibition as a promising microbiome-targeted therapeutic strategy for MASH.

CRediT AUTHORSHIP CONTRIBUTION STATEMENT

Wenchao Wei: Writing — review & editing, Writing — original draft, Visualization, Investigation, Formal analysis. **Radka Graf:** Supervision, Methodology, Formal analysis, Conceptualization. **Yanhan Wang:** Investigation. **Christopher J. Oalmann:** Supervision, Resources, Project administration, Methodology, Conceptualization. **Jennifer T. Lau:** Supervision, Project administration, Conceptualization. **Xinyi Wang:** Formal analysis, Data curation. **Melanie Chien:** Methodology, Formal analysis. **Mary C. Conrad:** Conceptualization. **Jonah Simon:** Methodology, Formal analysis. **Souradipta Ganguly:** Methodology, Investigation. **Tomoo Yamazaki:** Investigation. **Aenne Harberts:** Investigation. **Sainan Chen:** Investigation. **Marcos F. Fondevila:** Investigation. **Debanjan Dhar:** Investigation. **A. Stewart Campbell:** Writing — review & editing, Supervision, Resources, Project administration, Funding acquisition, Formal analysis, Conceptualization. **Rebecca K. Senter:** Writing — review & editing, Supervision, Resources, Project administration, Funding acquisition, Formal analysis, Conceptualization. **Bernd Schnabl:** Writing — review & editing, Supervision, Resources, Project administration, Investigation, Funding acquisition, Formal analysis, Conceptualization.

ETHICS DECLARATION

This study was conducted in accordance with the ARRIVE (Animal Research: Reporting of In Vivo Experiments) guidelines. This study was approved by the UC San Diego Institutional Animal Care and Use Committee (IACUC).(Approval No. S09042).

DECLARATION OF GENERATIVE AI AND AI-ASSISTED TECHNOLOGIES

The authors used ChatGPT (OpenAI) to assist with language editing and clarity of expression. No content generation, data analysis, or scientific interpretation was performed by the tool. All content was reviewed and approved by the authors.

DECLARATION OF COMPETING INTERESTS

B.S. has been consulting for Boehringer Ingelheim Pharma and Mabwell Therapeutics (prior 24 months). B.S.'s institution UC San Diego has received research support from Vertero Therapeutics (formerly Axial Therapeutics), Apollo Therapeutics, ChromoLogic, Intercept Pharmaceuticals and Prodigy Biotech (prior 24 months). B.S. is founder of Nterica Bio. UC San Diego has filed several patents with B.S. as inventor related to this work. R.G., C.J.O, J.T.L, M.C., M.C.C., J.S., A.S.C. and R.K.S. are or were employees of Vertero Therapeutics (formerly Axial Therapeutics).
All other authors declare that they have no known competing financial interests or personal relationships that could have appeared to influence the work reported in this paper.

ACKNOWLEDGMENTS

This study was supported by a lab service agreement with Vertero Therapeutics (formerly Axial Therapeutics) and services provided by NIH center P30 DK120515. We thank Dr. Sloan Devlin for helpful discussions related to this work.

APPENDIX A. SUPPLEMENTARY DATA

Supplementary data to this article can be found online at https://doi.org/10.1016/j.molmet.2026.102430.

DATA AVAILABILITY

Data will be made available on request.

REFERENCES

[1] Targher G, Valenti L, Byrne CD. Metabolic dysfunction-associated steatotic liver disease. N Engl J Med 2025;393:683—98. https://doi.org/10.1056/NEJMra2412865.
[2] Stefan N, Yki-Jarvinen H, Neuschwander-Tetri BA. Metabolic dysfunction-associated steatotic liver disease: heterogeneous pathomechanisms and effectiveness of metabolism-based treatment. Lancet Diabetes Endocrinol 2025;13:134—48. https://doi.org/10.1016/S2213-8587(24)00318-8.
[3] Tilg H, Petta S, Stefan N, Targher G. Metabolic dysfunction-associated steatotic liver disease in adults: a review. JAMA 2026;335:163—74. https://doi.org/10.1001/jama.2025.19615.
[4] Tiwari A, Sharma A, Kumar H, Gupta V, Deshpande V, Mupparaju JS, et al. Resmetirom for MASH: a comprehensive review of a novel therapeutic frontier. Biomedicines 2025;13. https://doi.org/10.3390/biomedicines13092079.
[5] Harrison SA, Bedossa P, Guy CD, Schattenberg JM, Loomba R, Taub R, et al. A phase 3, randomized, controlled trial of resmetirom in NASH with liver fibrosis. N Engl J Med 2024;390:497—509. https://doi.org/10.1056/NEJMoa2309000.
[6] Sanyal AJ, Newsome PN, Kliers I, Ostergaard LH, Long MT, Kjaer MS, et al. Phase 3 trial of semaglutide in metabolic dysfunction-associated steatohepatitis. N Engl J Med 2025;392:2089—99. https://doi.org/10.1056/NEJMoa2413258.
[7] Sayin SI, Wahlstrom A, Felin J, Jantti S, Marschall HU, Bamberg K, et al. Gut microbiota regulates bile acid metabolism by reducing the levels of tauro-beta-muricholic acid, a naturally occurring FXR antagonist. Cell Metab 2013;17:225—35. https://doi.org/10.1016/j.cmet.2013.01.003.
[8] Jiao N, Baker SS, Chapa-Rodriguez A, Liu W, Nugent CA, Tsompana M, et al. Suppressed hepatic bile acid signalling despite elevated production of primary and secondary bile acids in NAFLD. Gut 2018;67:1881—91. https://doi.org/10.1136/gutjnl-2017-314307.
[9] Fleishman JS, Kumar S. Bile acid metabolism and signaling in health and disease: molecular mechanisms and therapeutic targets. Signal Transduct Targeted Ther 2024;9:97. https://doi.org/10.1038/s41392-024-01811-6.
[10] Jia W, Wei M, Rajani C, Zheng X. Targeting the alternative bile acid synthetic pathway for metabolic diseases. Protein Cell 2021;12:411—25. https://doi.org/10.1007/s13238-020-00804-9.

 Published by Elsevier GmbH. This is an open access article under the CC BY license (http://creativecommons.org/licenses/by/4.0/).

[11] Takahashi S, Fukami T, Masuo Y, Brocker CN, Xie C, Krausz KW, et al. Cyp2c70 is responsible for the species difference in bile acid metabolism between mice and humans. J Lipid Res 2016;57:2130–7. https://doi.org/10.1194/jlr.M071183.

[12] Fuchs CD, Simbrunner B, Baumgartner M, Campbell C, Reiberger T, Trauner M. Bile acid metabolism and signalling in liver disease. J Hepatol 2025;82:134–53. https://doi.org/10.1016/j.jhep.2024.09.032.

[13] Jia B, Park D, Hahn Y, Jeon CO. Metagenomic analysis of the human microbiome reveals the association between the abundance of gut bile salt hydrolases and host health. Gut Microbes 2020;11:1300–13. https://doi.org/10.1080/19490976.2020.1748261.

[14] Jiao N, Loomba R, Yang ZH, Wu D, Fang S, Bettencourt R, et al. Alterations in bile acid metabolizing gut microbiota and specific bile acid genes as a precision medicine to subclassify NAFLD. Physiol Genom 2021;53:336–48. https://doi.org/10.1152/physiolgenomics.00011.2021.

[15] Smirnova E, Muthiah MD, Narayan N, Siddiqui MS, Puri P, Luketic VA, et al. Metabolic reprogramming of the intestinal microbiome with functional bile acid changes underlie the development of NAFLD. Hepatology 2022;76:1811–24. https://doi.org/10.1002/hep.32568.

[16] Jones EV, Wang Y, Wei W, Reed JC, Chaudhari SN, Li DK, et al. Bile salt hydrolase activity as a rational target for MASLD therapy. Gut Microbes 2026;18:2608437. https://doi.org/10.1080/19490976.2025.2608437.

[17] Yao L, Seaton SC, Ndousse-Fetter S, Adhikari AA, DiBenedetto N, Mina AI, et al. A selective gut bacterial bile salt hydrolase alters host metabolism. eLife 2018;7. https://doi.org/10.7554/eLife.37182.

[18] Li DK, Chaudhari SN, Lee Y, Sojoodi M, Adhikari AA, Zukerberg L, et al. Inhibition of microbial deconjugation of micellar bile acids protects against intestinal permeability and liver injury. Sci Adv 2022:8. https://doi.org/10.1126/sciadv.abo2794. eabo2794.

[19] Ganguly S, Muench GA, Shang L, Rosenthal SB, Rahman G, Wang R, et al. Nonalcoholic steatohepatitis and HCC in a hyperphagic mouse accelerated by Western diet. Cell Mol Gastroenterol Hepatol 2021;12:891–920. https://doi.org/10.1016/j.jcmgh.2021.05.010.

[20] Arsov T, Larter CZ, Nolan CJ, Petrovsky N, Goodnow CC, Teoh NC, et al. Adaptive failure to high-fat diet characterizes steatohepatitis in Alms1 mutant mice. Biochem Biophys Res Commun 2006;342:1152–9. https://doi.org/10.1016/j.bbrc.2006.02.032.

[21] Pradeau M, Beaulieu S, Paquet V, Trottier J, Verreault M, Ferland S, et al. Plasma and fecal bile acids profiles in metabolic dysfunction-associated steatotic liver disease with advanced fibrosis. Am J Physiol Endocrinol Metab 2025;329:E644–54. https://doi.org/10.1152/ajpendo.00346.2024.

[22] Adhikari AA, Seegar TCM, Ficarro SB, McCurry MD, Ramachandran D, Yao L, et al. Development of a covalent inhibitor of gut bacterial bile salt hydrolases. Nat Chem Biol 2020;16:318–26. https://doi.org/10.1038/s41589-020-0467-3.

[23] Huang F, Zheng X, Ma X, Jiang R, Zhou W, Zhou S, et al. Theabrownin from Pu-erh tea attenuates hypercholesterolemia via modulation of gut microbiota and bile acid metabolism. Nat Commun 2019;10:4971. https://doi.org/10.1038/s41467-019-12896-x.

[24] Smith K, Zeng X, Lin J. Discovery of bile salt hydrolase inhibitors using an efficient high-throughput screening system. PLoS One 2014;9:e85344. https://doi.org/10.1371/journal.pone.0085344.

[25] Seo KH, Bartley GE, Tam C, Kim HS, Kim DH, Chon JW, et al. Chardonnay grape seed flour ameliorates hepatic steatosis and insulin resistance via altered hepatic gene expression for oxidative stress, inflammation, and lipid and ceramide synthesis in diet-induced Obese mice. PLoS One 2016;11:e0167680. https://doi.org/10.1371/journal.pone.0167680.

[26] Wang DQ, Tazuma S, Cohen DE, Carey MC. Feeding natural hydrophilic bile acids inhibits intestinal cholesterol absorption: studies in the gallstone-susceptible mouse. Am J Physiol Gastrointest Liver Physiol 2003;285:G494–502. https://doi.org/10.1152/ajpgi.00156.2003.

[27] Liu J, Lu H, Lu YF, Lei X, Cui JY, Ellis E, et al. Potency of individual bile acids to regulate bile acid synthesis and transport genes in primary human hepatocyte cultures. Toxicol Sci 2014;141:538–46. https://doi.org/10.1093/toxsci/kfu151.

[28] de Boer JF, Verkade E, Mulder NL, de Vries, Huijkman N, Koehorst M, et al. A human-like bile acid pool induced by deletion of hepatic Cyp2c70 modulates effects of FXR activation in mice. J Lipid Res 2020;61:291–305. https://doi.org/10.1194/jlr.RA119000243.

[29] Gonzalez FJ, Jiang C, Patterson AD. An intestinal microbiota-farnesoid X receptor axis modulates metabolic disease. Gastroenterology 2016;151:845–59. https://doi.org/10.1053/j.gastro.2016.08.057.

[30] Brighton CA, Rievaj J, Kuhre RE, Glass LL, Schoonjans K, Holst JJ, et al. Bile acids trigger GLP-1 release predominantly by accessing basolaterally located G protein-coupled bile acid receptors. Endocrinology 2015;156:3961–70. https://doi.org/10.1210/en.2015-1321.

[31] Thomas C, Gioiello A, Noriega L, Strehle A, Oury J, Rizzo G, et al. TGR5-mediated bile acid sensing controls glucose homeostasis. Cell Metab 2009;10:167–77. https://doi.org/10.1016/j.cmet.2009.08.001.

[32] Wang Q, Lin H, Shen C, Zhang M, Wang X, Yuan M, et al. Gut microbiota regulates postprandial GLP-1 response via ileal bile acid-TGR5 signaling. Gut Microbes 2023;15:2274124. https://doi.org/10.1080/19490976.2023.2274124.

 Published by Elsevier GmbH. This is an open access article under the CC BY license (http://creativecommons.org/licenses/by/4.0/).